



UNIVERSITY OF LEEDS

This is a repository copy of *Pediatric Patient Surface Model Atlas Generation and X-Ray Skin Dose Estimation*.

White Rose Research Online URL for this paper:  
<http://eprints.whiterose.ac.uk/149280/>

Version: Accepted Version

---

**Proceedings Paper:**

Zhong, X, Roser, P, Bayer, S et al. (7 more authors) (2019) Pediatric Patient Surface Model Atlas Generation and X-Ray Skin Dose Estimation. In: Handels, H, Deserno, TM, Maier, A, Maier-Hein, KH, Palm, C and Tolxdorff, T, (eds.) Informatik aktuell. BVM 2019: Bildverarbeitung für die Medizin 2019, 17-19 Mar 2019, Lübeck, Germany. Springer Vieweg , pp. 122-127. ISBN 978-3-658-25325-7

[https://doi.org/10.1007/978-3-658-25326-4\\_27](https://doi.org/10.1007/978-3-658-25326-4_27)

---

© Springer Fachmedien Wiesbaden GmbH, ein Teil von Springer Nature 2019. This is a post-peer-review, pre-copyedit version of an article published in Informatik aktuell. The final authenticated version is available online at:  
[https://doi.org/10.1007/978-3-658-25326-4\\_27](https://doi.org/10.1007/978-3-658-25326-4_27). Uploaded in accordance with the publisher's self-archiving policy.

**Reuse**

Items deposited in White Rose Research Online are protected by copyright, with all rights reserved unless indicated otherwise. They may be downloaded and/or printed for private study, or other acts as permitted by national copyright laws. The publisher or other rights holders may allow further reproduction and re-use of the full text version. This is indicated by the licence information on the White Rose Research Online record for the item.

**Takedown**

If you consider content in White Rose Research Online to be in breach of UK law, please notify us by emailing [eprints@whiterose.ac.uk](mailto:eprints@whiterose.ac.uk) including the URL of the record and the reason for the withdrawal request.



[eprints@whiterose.ac.uk](mailto:eprints@whiterose.ac.uk)  
<https://eprints.whiterose.ac.uk/>

# Pediatric Patient Surface Model Atlas Generation and X-Ray Skin Dose Estimation

Xia Zhong<sup>1</sup>, Philipp Roser<sup>1,3</sup>, Siming Bayer<sup>1</sup>, Nishant Ravikumar<sup>1</sup>  
Norbert Strobel<sup>2</sup>, Annette Birkhold<sup>2</sup>, Tim Horz<sup>2</sup>, Markus Kowarschik<sup>2</sup>,  
Rebecca Fahrig<sup>2</sup>, Andreas Maier<sup>1,3</sup>

<sup>1</sup>Pattern Recognition Lab, FAU Erlangen-Nürnberg

<sup>2</sup>Siemens Healthcare GmbH, Forchheim Germany

<sup>3</sup>Erlangen Graduate School in Advanced Optical Technologies (SAOT)

xia.zhong@fau.de

**Abstract.** Fluoroscopy is used in a wide variety of examinations and procedures to diagnose or treat patients in modern pediatric medicine. Although these image guided interventions have many advantages in treating pediatric patients, understanding the deterministic and long term stochastic effects of ionizing radiation are of particular importance for this patient demographic. Therefore, quantitative estimation and visualization of radiation exposure distribution, and dose accumulation over the course of a procedure, is crucial for intra-procedure dose tracking and long term monitoring for risk assessment. Personalized pediatric models are necessary for precise determination of patient-X-ray interactions. One way to obtain such a model is to collect data from a population of pediatric patients, establish a population based generative pediatric model and use the latter for skin dose estimation. In this paper, we generate a population model for pediatric patient using data acquired by two RGB-D cameras from different views. A generative atlas was established using template registration. We evaluated the registered templates and generative atlas by computing the mean vertex error to the associated point cloud. The evaluation results show that the mean vertex error reduced from  $25.2 \pm 12.9$  mm using an average surface model to  $18.5 \pm 9.4$  mm using specifically estimated pediatric surface model using the generated atlas. Similarly, the dose estimation error was halved from  $10.6 \pm 8.5\%$  using the average surface model to  $5.9 \pm 9.3\%$  using the personalized surface estimates.

## 1 Introduction

In modern pediatric radiology, fluoroscopy is used to provide the physicians dynamic and functional information of the patients' internal organs, both in diagnostic and minimally invasive surgery. However, as an ionizing radiation based imaging modality, the use of fluoroscopy is associated with radiation related risks such as radiation-induced cancer. A retrospective study by Pearce [1] showed a noticeably increased risk of leukemia and brain cancer when accumulated dose reached a certain level in children. Therefore it is desirable to reduce

X-ray exposure adhering to the as low as reasonably achievable (ALARA) principle, particularly in pediatric patients, who are more sensitive to X-rays than adults. One way to help facilitate dose reduction in the interventional suite is to use digital patient twins to better model and monitor X-ray dose exposure. An interesting practical application for such models is to keep track of the dose deposition in the skin. Skin entrance dose estimation often comprises two steps: (1) identification of the irradiated skin area, and (2) dose calculation based on a forward projection of an online-measured dose-related quantity such as dose-area-product from the X-ray source onto the skin surface. Previous studies have shown progressive improvements concerning the accuracy of skin dose estimation, but also highlight the importance of an accurate patient model [2]. An interesting practical question is, how accurate a patient model has to be, such that the skin dose estimate is reliable. This forms the basic motivation for the current study, with the focus on pediatric patients. The associated task is challenging as the anatomy and physiology of children exhibits a significantly higher degree of variation relative to adults. Models of pediatric patients are typically generated using MRI (or in rare cases CT) scans, referred to as computation or reference phantoms. While such phantoms are highly detailed and accurate, they are difficult to obtain on a large scale as they usually require very high resolution data and significant manual post-processing, e.g. for segmentation. With the introduction of RGB-D cameras, using depth data to construct surface models has become increasingly popular. While most efforts have been aimed at modeling adults [3,4,5], Hesse et al. [6] investigated methods to generate infant body models, using RGB-D image sequences.

In this work, we propose a method to build a generative atlas using two RGB-D cameras. Using this atlas, a patient specific pediatric model can be estimated using patient height and weight as input data. We evaluated the model both in terms of model estimation accuracy, and its impact on skin dose estimation.

## 2 Materials and Methods

**RGBD imaging setup and data acquisition.** Two Microsoft Kinect V2 cameras were used to acquire RGBD data from two fixed, but different viewing angles. Children ( $n=20$ ) were asked to stand in front of a wall in the target region of interest (ROI). Cameras were mounted on two tripods and oriented such that the target ROI (complete child) was located in the ISO center. The angle between the two cameras was set to be approximately  $30^\circ$ . An illustration of the acquisition setup is shown in Fig. 1, left side. The RGBD cameras are calibrated jointly using a calibration phantom to determine distortion correction and obtain the intrinsic as well as the extrinsic camera parameters. Besides the RGBD data, we further collected meta data (gender, height, weight and age) of the children. In order to get most accurate height and weight information, measurements were performed shortly before the image acquisition. Gender and age of the children was inquired from the parents. The data acquisition was voluntary and followed the rules set out by the European General Data Protection Regulation. Each

data set acquired and processed has an associated consent form with signatures of both parents and the child, if necessary.

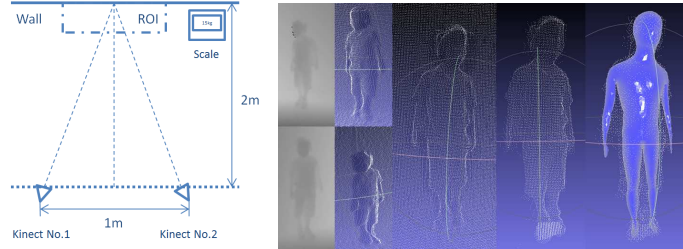


**Fig. 1.** Data acquisition setup (left) and processing pipeline (right).

**Preprocessing.** The data preprocessing pipeline is illustrated in Fig. 1. First, the point cloud of a patient is reconstructed using both depth images from the two cameras. Two point clouds are reconstructed separately using associated undistorted depth images and the intrinsic camera matrix. These two point clouds are then aligned using the extrinsic camera matrices. As the tripods may have moved accidentally during the acquisition, we added an extra correction step performing a rigid registration using coherent point drift (CPD) [7] to ensure that the point clouds are aligned. Subsequently, the two point clouds of each child are merged. Next, we determined the wall and floor planes using RANSAC with plane fitting and removed these from the data. As the backs of the patients and the bottom of their feet were occluded in the acquisition setup, we used the calculated wall and floor planes to fill in the missing information. As not all patients were positioned next to the wall, we had to manually align the reference wall planes to obtain the missing data. Finally, we manually removed remaining artifacts, e.g., wide clothes obstructing the body silhouette. The extracted region was adjusted for cases where patients were positioned outside the target ROI.

**Template fitting.** Template fitting was used to extract a structured mesh for each preprocessed point cloud, for atlas generation. The MakeHuman<sup>1</sup> software was used to initialize a patient *reference* template. An iterative scheme was then used to fit the *reference* to the cleaned-up point cloud. In each iteration, the *reference* was registered to each point cloud using an affine, and subsequently, non-rigid transformation (using CPD). As clothing and pose of the children varied significantly in the training data, a high outlier rate was used in the CPD registration. CPD tries to find a globally optimal solution when fitting the template to the point cloud by performing a non-rigid deformation. Since the head-to-body-ratio of children, however, changes with age, we decided to treat head and body trunk separately.

<sup>1</sup> <http://www.makehumancommunity.org/>

Afterwards, the *reference* was again fitted to the separately registered point clouds to ensure smoothness of the model. At the end of each iteration, the *reference* was updated by calculating the mean shape of all fitted meshes. This fitting process converged after a few iterations, and we took the result for each point cloud as the associated *ground truth* mesh.

**Atlas generation.** The goal of atlas generation is to learn a generative model and estimate a personalized surface, based on a given height and weight of the child. For this purpose, we used the *ground truth* meshes to compute a statistical shape model using Principal Component Analysis (PCA), where  $\mathbf{P}^c$  encodes the modes of variation and  $\mathbf{b}_i^c$  encodes the associated shape parameters. We then computed the PCA space of the associated height and weight data. Unfortunately, the measured data in the acquired datasets suffered from rank deficiency, making a regression of shape parameters  $\mathbf{b}_i^c = \mathbf{f}(h_i, w_i)$  in native PCA space insufficient to generate a model having correct height  $h_i$  and weight  $w_i$ . Therefore, we used the mode of variation  $\mathbf{P}^a$  learned from the adult CEASAR [8] database as an extra term. Our aim was to find the associated shape parameters  $\mathbf{b}^a$  for a given height  $h_i$  and weight  $w_i$  such that

$$\mathbf{x}_i = \bar{\mathbf{x}} + \mathbf{P}^c \mathbf{b}_i^c + \mathbf{P}^a \mathbf{b}_i^a \quad (1)$$

$$\arg \min_{\mathbf{b}^a} = \sum_i (\lambda_1 \|\rho V(\mathbf{x}_i) - w_i\| + \lambda_2 \|H(\mathbf{x}_i) - h_i\|) + \|\nabla \mathbf{b}^a\| \quad (2)$$

where  $\rho$  denotes the approximate body mass density of children,  $V(\cdot)$  describes the calculation of the input mesh volume, and  $H(\cdot)$  represents the calculation of the height of the input mesh, respectively. The gradient of the shape parameter ensures smooth adaption. Minimizing this equation resulted in generation of an *estimated* surface model which is in good agreement with the *ground truth* and coherent with the associated measured data.

**Skin Entrance Dose Estimation.** For validation purposes, we computed the accumulated skin entrance dose for each surface model, focused on a central body region. The goal was not to simulate an actual interventional setup, but to focus on differences in skin dose estimation resulting from the use of different models. The surface models were placed within a virtual model of the imaging setup (source - object - detector) for the dose simulations, comprising a homogeneous projection and view geometry of the X-ray source and the model matrix of the patient, specifying its orientation and position with respect to the X-ray beam. Based on the resulting model-view-projection matrix, each mesh face was forward projected onto the detector plane if at least one associated vertex was positioned within the X-ray beam and the face normal pointed towards the X-ray source making sure that only those surfaces were considered that received radiation. The corresponding distance to the X-ray source was given by the last homogeneous coordinate of each vertex. Applying barycentric depth interpolation, the triangle in the image plane was rasterized and the depth map was constructed iteratively [9]. The skin entrance dose was then calculated by forward projecting a dose-related quantity measured at the X-ray emitter onto the area of irradiation, taking additional correction terms into account [2]. We eval-

uated the percentage error of the skin entrance dose introduced by both surface estimation methods: 1) using an average surface model, 2) using personalized surface models. Both types of surface models were based on the atlas data. The template fitted to the original point cloud served as ground truth.

### 3 Evaluation and Results

In total, we gathered 20 point cloud sets with associated measurements. We first evaluated the accuracy of the atlas generation pipeline by overlaying the atlas-based *estimate* with the associated 3D point cloud and calculating the minimal distance for each vertex. We performed a leave-one-out cross validation in which the *estimate* was rigidly registered to the associated point cloud using CPD. An illustration of color coded mean vertex error of the *reference*, *estimate* and *ground truth*, is shown in Fig. 2. Using only the *reference*, an average distance of  $25.2 \pm 12.9$  mm was achieved. The *ground truth* had an average distance of  $15.3 \pm 8.7$  mm. A mean vertex error of  $18.5 \pm 9.4$  mm was achieved using the *estimate*. The percentage error of the skin entrance dose using the template model (for each sample compared to its ground truth) was estimated to  $10.6 \pm 8.5$  %. The percentage error using models generated by the atlas (for each sample compared to its ground truth) was  $5.9 \pm 9.3$  %.

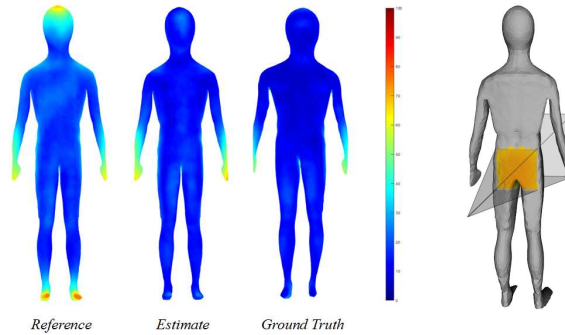


**Fig. 2.** An illustration of mean vertex distance in mm to its merged point cloud using the reference template late (left), estimation based on metadata (middle) and the fitted template. Right: Visualization of dose estimation setup.

### 4 Discussion

The proposed statistical atlas complements our adult atlas derived from the CEASAR database. Both atlases yield comparable accuracy. Although the average error of approximately 2 cm will still contribute to a (skin) dose estimation

error, the proposed atlas is still an improvement when compared to a setup involving only one single representation, (average) reference model, for all pediatric cases. Our statistical atlas could also be used as a first estimate of a continuously adapting model which refines itself after each new source of information, e.g., provided by successive MRI scans. A possible improvement of the modeling pipeline would be to use a more robust point set registration method than CPD. Although CPD introduces an outlier ratio, the underlying Gaussian mixture model can not effectively model the point cloud in the presence of extreme or large percentage of outliers. Despite the successful application of the adults' modes of variation to the children's atlas, more representative modes of variation of the children might improve the accuracy of the model further. In this atlas, we used height and weight measurements only. We were not able to account for gender and age of the children due to the rank deficiency in the dataset. This was caused by the limited amount of training data collected. In future work, we hope to be able to gather more data such that we can incorporate this information as well, to further reduce the estimation error.

**Acknowledgements** We gratefully acknowledge the support of Siemens Healthineers, Forchheim, Germany. Note that the concepts and information presented in this paper are based on research, and they are not commercially available.

## References

1. Pearce MS, et al. Radiation exposure from CT scans in childhood and subsequent risk of leukaemia and brain tumours: a retrospective cohort study. *The Lancet*. 2012;380(9840):499–505.
2. Johnson PB, et al. Skin dose mapping for fluoroscopically guided interventions. *Med Phys*. 2011;38(10):5490–5499.
3. Zhong X, et al. Generation of Personalized Computational Phantoms Using Only Patient Metadata. In: IEEE, editor. 2017 IEEE Nuclear Science Symposium and Medical Imaging Conference Record (NSS/MIC); 2017. .
4. Zhong X, et al. A machine learning pipeline for internal anatomical landmark embedding based on a patient surface model. *Int J Comput Assist Radiol Surg*. 2018;10:1–9.
5. Wu Y, et al. Towards Generating Personalized Volumetric Phantom from Patients' Surface Geometry. In: *Med Image Comput Comput Assist Interv*. Springer; 2018. p. 171–179.
6. Hesse N, et al. Learning an Infant Body Model from RGB-D Data for Accurate Full Body Motion Analysis. In: *Med Image Comput Comput Assist Interv*. Springer; 2018. p. 792–800.
7. Myronenko A, Song X. Point set registration: Coherent point drift. *IEEE Trans Pattern Anal Mach Intell*. 2010;32(12):2262–2275.
8. Robinette KM, et al. The CAESAR project: a 3-D surface anthropometry survey. In: *3-D Digital Imaging and Modeling*. IEEE; 1999. p. 380–386.
9. Catmull E. A subdivision algorithm for computer display of curved surfaces. Utah University Salt Lake city school of computing; 1974.